





Open Archive Toulouse Archive Ouverte (OATAO)

OATAO is an open access repository that collects the work of Toulouse researchers and makes it freely available over the web where possible

This is an author's version published in: <http://oatao.univ-toulouse.fr/24655>

Official URL: <https://doi.org/10.1016/j.electacta.2019.01.184>

To cite this version:

Wang, Mengying and Barnabé, Antoine  and Thimont, Yohann  and Wang, Jinmin and He, Yingchun and Liu, Qirong and Zhong, Xiaolan and Dong, Guobo and Yang, Jiaming and Diao, Xungang *Optimized properties of innovative ElectroChromic Device using ITO / Ag / ITO electrodes.* (2019) *Electrochimica Acta*, 301. 200-208. ISSN 0013-4686

Any correspondence concerning this service should be sent to the repository administrator: tech-oatao@listes-diff.inp-toulouse.fr

Optimized properties of innovative ElectroChromic Device using ITO / Ag / ITO electrodes

Mengying Wang ^{a, b}, Antoine Barnabé ^c, Yohann Thimont ^c, Jinmin Wang ^d, Yingchun He ^a, Qirong Liu ^a, Xiaolan Zhong ^a, Guobo Dong ^a, Jiaming Yang ^a, Xungang Diao ^{e, *}

^a School of Physics Science and Nuclear Energy Engineering, Beihang University, Beijing, 100191, PR China

^b Shen Yuan Honors College, Beihang University, Beijing, 100191, PR China

^c CRIMAT, Université de Toulouse, CNRS, Université Toulouse 3 Paul Sabatier, 118 route de Narbonne, 31062 Toulouse Cedex 9, France

^d School of Environmental and Materials Engineering, College of Engineering, Shanghai Polytechnic University, Shanghai, 201209, PR China

^e School of Energy and Power Engineering, Beihang University, Beijing, 100191, PR China

ARTICLE INFO

Keywords:

Transparent conductive materials
Multilayer
Electrochromic characteristics
Polymer gel electrolyte
Electrochromic devices

ABSTRACT

The “Dielectric/Metal/Dielectric” (DMD) stacked films being used as transparent and conductive (TC) electrodes, have demonstrated excellent application in the ElectroChromic (EC) process and devices. In this work, multilayers (IAI) made of 50 nm of Indium Tin Oxide (ITO)/5 nm of metallic silver (Ag)/30 nm of ITO that exhibit band gap, low resistance of 7.4 Ω and the high figure of merit of $9.9 \times 10^{-3} \Omega^{-1}$ were introduced in a complete five layer Glass/IAI/NiO_x/LiClO₄ PC PMMA/WO₃/IAI/Glass ElectroChromic Device (ECD). The single IAI electrode as well as the two active EC layers Glass/IAI/NiO_x and Glass/IAI/WO₃ were firstly characterized for their TC and EC properties respectively. Then, the EC properties of the complete five layer ECD were analyzed. Fast response time (2.02 s for the bleaching and 2.25 s for complete coloration), wide optical modulation in the visible light region (~55% at 550 nm), long lifetime (more than 6000 s), large capacity and good stability as well as high coloration efficiency (31.7 cm² C⁻¹) were obtained. The improved EC performance of ECD were related to the good electrical and optical properties of IAI electrode.

1. Introduction

ElectroChromic Devices (ECD), which can switch between the transparent bleaching state and the dark coloring state in a continual but reversible manner on application of voltage, have attracted much attention as the promising part of the smart windows [1–4]. The most typical and accepted structure of ECD is a five layer stack of electrode/ion storage layer/electrolyte/electrochromic layer/top electrode [4]. Each of the component of this full ECD plays an important role in the overall electrochromic properties.

The Transparent Conductive Oxides (TCO) which are the main constitutive materials of the top and bottom electrode of the ECD need to have optimized opto electrical properties [1–12]. Transparent conductive electrode material is probably the most expensive part of the ECD. Indium Tin Oxide (ITO) and Aluminum doped

Zinc Oxide (AZO) [13], due to their two main opto electrical properties (electrical conductivity and optical transparency), as well as their ability to be deposited as thin films. Generally, the balance of the optimal optical and electrical properties is difficult to realize because these two properties are usually mutually exclusive, and the overall conductivity of the wide band gap oxide semiconducting material is somehow limited. To solve this problem, the use of extra thin metallic films in a composite multilayer stack is an interesting alternative to ITO or AZO. The structure of this transparent conductive stack is “dielectric/metal/dielectric” (DMD) triple layer. Such DMD composite multilayer stacks composed of few nanometers of Ag or Au, could exhibit much lower conductivities than the single ITO film while maintaining good optical properties [14].

The recent development of the DMD structures have a broad application prospect, but the use as the electrode in ECD should be expanded. Jeong J. A. and Kim H. K [15], fabricated the low resistance and highly transparent ITO/Ag/ITO multilayer electrode using surface plasmon resonance of Ag layer for bulk heterojunction

* Corresponding author.

E-mail address: diaoxg@buaa.edu.cn (X. Diao).

organic solar cells. Boscarino S. et al. [16] deposited ITO/Ag/ITO and AZO/Ag/AZO triple layers with resistivity of around $10^{-5} \Omega$ and over 80% transmittance in the visible range for photovoltaic applications. Li H. et al. [17] studied the ITO free $\text{WO}_3/\text{Ag}/\text{WO}_3$ triple layers which were as both transparent electrodes and electrochromic materials. These ECD have the long term cycling stability (3000 cycles) and short switching time (coloration time ~ 11 s; bleaching time ~ 10.5 s). MoO_3 films have also been studied as the DMD structure electrodes in the electrochromic process and devices: Liu, Y. et al. [18] have achieved the high performance ITO free ECD based on $\text{MoO}_3/\text{Ag}/\text{MoO}_3$ films with faster response time, better optical contrast and higher coloration efficiency than the common MoO_3 on ITO. Thereafter, Dong, W. et al. [19] has achieved superior optical and electrochromic properties by introducing $\text{MoO}_3/\text{WO}_3/\text{Ag}/\text{MoO}_3$ WO_3 films in the ECD.

According to the electrolyte, the ECD are divided into two types: (I) all thin film solid state inorganic ECD with a transport ionic conductive inorganic films as the electrolyte (H^+ , Li^+ and other small cationic ions) [1,4,5,20]; (II) all solid state inorganic/organic ECD with a polymer gel electrolyte, for instance, polymethyl methacrylate (PMMA PC LiClO_4) [21,22], poly (3, 4 ethylenedioxythiophene):poly (styrenesulfonate)/Si (PETOD:PSS) [23], viologen [24],

Nickel oxide (NiO_x) and tungsten oxide (WO_3) are the most extensively studied electrochromic materials for ECD as the ion storage layer and the electrochromic layer, respectively [1–5,20–25].

In this work, we have deposited by reactive DC magnetron sputtering on glass ITO/Ag/ITO (IAI) multilayer films with improved optical and electrical properties. The extra thin Ag layers (5 nm) are inserted between the top ITO films (50 nm) and bottom ITO films (30 nm). Active electrochromic materials NiO_x and WO_3 were then deposited on the transparent and conductive IAI electrode before being laminated with polymethyl methacrylate PMMA PC LiClO_4 as the electrolyte to finally form the complete five layer ECD. TC and EC properties were systematically studied at various step of the elaboration of the ECD. In this work, the EC properties of a new all solid state ECD elaborated with optimized IAI electrodes are studied.

2. Experiment details

2.1. Fabrication of ECD

Transparent and conductive multilayer IAI films were deposited on glass substrates by DC reactive magnetron sputtering at room temperature. Before the whole process of the experiment, the glass substrates were successively cleaned in ethanol solution and deionized water for 20 min with the ultrasonic wave cleaning machine. The substrates were then placed into the vacuum chamber and targets were pre sputtered with pure Ar atmosphere for 5 min to remove the pollution. The ultimate vacuum of 1×10^{-4} Pa in the chamber is obtained by using a molecular pump. The sputtered gas was a mixture of O_2 (99%) and Ar (99.99%), and their flow rate were separately controlled by mass flow controllers. The bottom ITO layer was first deposited onto the glass substrates by employing the ITO target (composition of 10 %wt. SnO_2 and 90 %wt. In_2O_3). After the bottom layer being deposited, the intermediate Ag layer was continuously sputtered onto the bottom ITO layer without breaking the vacuum with an Ag metal target (purity 99.99%). Next, the top ITO layer was deposited under the same conditions as the bottom layer. The ITO film thickness was controlled by the deposition time and the sample holder was kept rotating during the sputtering to ensure the film thickness uniformity.

The typical five layer ECD of Glass/IAI/ $\text{NiO}_x/\text{LiClO}_4$ PC PMMA/ $\text{WO}_3/\text{IAI}/\text{Glass}$ were fabricated in several steps: First, the single NiO_x and WO_3 films were deposited by the DC sputtering at room

temperature onto two pieces of IAI layers leading to Glass/IAI/ NiO_x on the one side and Glass/IAI/ WO_3 on the other one. The deposition parameters were summarized in Table 1. In parallel, the polymer gel electrolyte consisted of propylene carbonate (PC, AR), lithium perchlorate (LiClO_4 , AR) and polymethyl methacrylate (PMMA, AR). After all the work have been ready, the ECD was assembled in a vacuum autoclave regulated at 80°C constant temperature and 0.1 MPa constant pressure. The process of the fabrication and the entire ECD structure was shown in Fig. 1.

2.2. Characterization

The crystal structural properties of the samples were analyzed by Grazing Incidence X ray diffraction (GI XRD) and X Ray Reflectivity (XRR) using a Bruker AXS D8 Advance X ray diffractometer equipped with a copper source ($\lambda_{\text{CuK}\alpha 1}$ 1.5405 Å and $\lambda_{\text{CuK}\alpha 2}$ 1.5445 Å), a Gobel mirror and Bruker LynxEye detector used in OD/1D mode. The GI XRD data recorded with a grazing incidence angle of 1° were analyzed with the Bruker EVA software, JC PDF database and refined with the Rietveld method implemented in the FullProf Suite program. The XRR data were treated with the Bruker LEPTOS software.

The surface morphologies including the cross section were characterized by Scanning Electron Microscopy (SEM) using a Field Emission Gun FEG SEM (JEOL JSM 7800 F Prime) and FEG SEM/FIB apparatus (FEI Helios Nanolab600i dual beam). Atomic Force Microscopy (AFM) was also carried out using a Veeco Dimension 3100 instrument. The optical transmittance and reflectance spectra were collected in the 300–1100 nm wavelength range with a Bentham PVE 300 integrated spectrometer. The Total Transmission (TT) and Total Reflectance (TR) spectra of the sample were modeled using the SCOUT software (see details in Supporting Information) [26].

Accurate thickness of each layer was determined by the cross section SEM analysis and comforted by the XRR and optical data treatments.

The electrical resistivity measurements were performed at room temperature with the standard four point probe method (Signatone, USA).

The simultaneous test of the cyclic voltammograms (CV) and chronoamperometry (CA) were achieved by the conventional three electrodes configuration on a Chen Hua Instruments CHI 660E electrochemical workstation. The NiO_x and WO_3 coatings were all measured in the 1 mol/L PC LiClO_4 with scan rate of 50 mV/s. Ag/AgCl was applied as reference electrode and Pt sheet as the counter electrode. The applied potential was from -0.5 V to 1.5 V for NiO_x films and from -1.0 V to 1.5 V for WO_3 films. As for ECD, the potential ranged from ± 0.5 V to ± 2.0 V.

In situ optical transmittance with the wavelength ranging from 340 nm to 1100 nm at the room temperature and normal ambient air, was carried out with a Hitachi UV–Vis U 3010 spectrometer.

3. Results and discussion

3.1. Characterization of the IAI layer

The GI XRD measurement of the IAI layer clearly shows some

Table 1
The deposition parameters of the multilayer IAI films and electrochromic layers.

Target	Layer	Ar: O_2	Pressure (Pa)	Power (W)	Thickness (nm)
ITO	Top/Bottom	270:10	0.3	200	50/30
Ag	Ag	300:0	0.3	180	5
Ni	NiO_x	400:35	1.5	250	~ 150
W	WO_3	300:100	2.0	300	~ 610

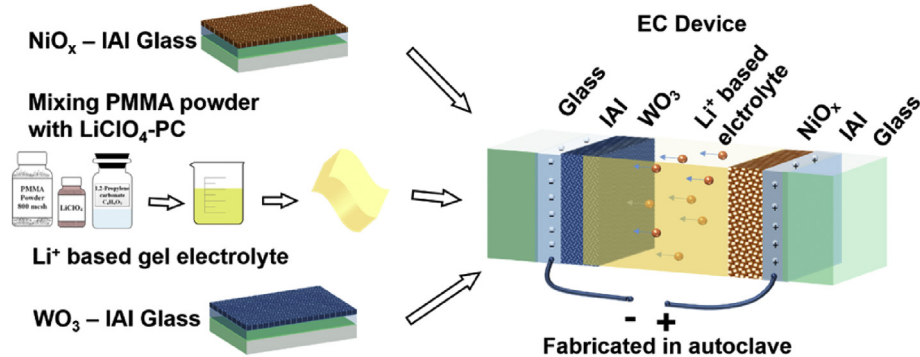


Fig. 1. Schematic schemes of the polymer gel electrolyte synthesis pathway and assemble process of the all-solid-state electrochromic devices with its entire typical structure.

broad peaks which belong to the ITO top layer in addition to the contribution of the amorphous substrate (Fig. 2 (a)). The characteristic peaks of the ITO phase were confirmed by an extra GI XRD analysis carried out on a 350 °C post annealed sample (shown in the Supporting Information). Besides the Bragg peaks corresponding to the ITO phase, one very small additional peak is visible at around 38.2° in the 2θ range. This peak corresponds to the metallic silver (111) Bragg peak. This peak is very small and broad due to the limited thickness and size of the silver particles.

By fitting the thickness, roughness and density of the Glass/ITO/Ag/ITO multilayer system, a good fit of the XRR curve could be obtained as shown in Fig. 2 (b). Very low roughness ($R_a \approx 0.8 \text{ nm}$) comparable to the values deduced from AFM analysis ($R_a \approx 0.77 \text{ nm}$) and densities ($\rho_{\text{ITO}} \approx 6.2 \text{ g/cm}^3$ and $\rho_{\text{Ag}} \approx 9.5 \text{ g/cm}^3$) slightly smaller but close to the theoretical ones ($\rho_{\text{ITO}} \approx 7.1 \text{ g/cm}^3$ and $\rho_{\text{Ag}} \approx 10.5 \text{ g/cm}^3$) were deduced. Thicknesses of 27, 5 and 53 nm were obtained for, respectively, the bottom ITO, Ag and top ITO layers. These thicknesses are confirmed by the SEM cross section views (Fig. 2 (c)) with 50 and 30 nm from, respectively, the bottom and the top ITO layers. According to the measurement, the average thickness of the Ag layer is around 5 nm. One can note that the sputtered top ITO film is amorphous, dense, homogeneous and smooth (see the SEM and AFM in Fig. S1.). Similarly, to the pure ITO

films [27], the smooth surface of IAI films could contribute to the good electrical properties and avoid optical haze effect. Characteristic Bragg peak in GI XRD, contrast in SEM/compo mode and electron densities in XRR measurements all confirm that the silver is only present in its nanoparticle metallic form, i.e. is not oxidized during the deposition step.

A sample stack structure (glass/ITO/Ag/ITO) was employed to model TT and TR spectra. A good match between experimental and simulated TT and TR spectra was obtained with a standard deviation of 1.7×10^{-4} and 3.1×10^{-5} , respectively. The experimental and simulated TT, TR spectra are reported in Fig. 3 using, respectively, empty black and colored filled marks. Imported dielectric functions were used for the glass substrate and the Ag layers. Various dielectric models were used for both ITO layers (see Supporting Information for details). The KKR OJL2 [28] model allowed to deduce precisely the ITO band gap of 4.05 eV without any influence of the substrate and the Ag layer. The extended Drude model allowed to determine the plasma frequency of 12171 cm^{-1} which corresponds to a carrier density of $n = 4.96 \times 10^{20} \text{ cm}^{-3}$. From these models, an average value of the carrier mobility ($\mu = 2.7 \text{ cm}^2/\text{V}/\text{sec}$), electrical conductivity ($\sigma = 214 \text{ S cm}^{-1}$) as well as the n and k optical indexes of ITO layer (see Fig. 3 (b)) could be deduced. All these values agree with the classical experimental values reported in the literature for ITO [29,30]. The layer thicknesses of each film could also be obtained. They correspond to a

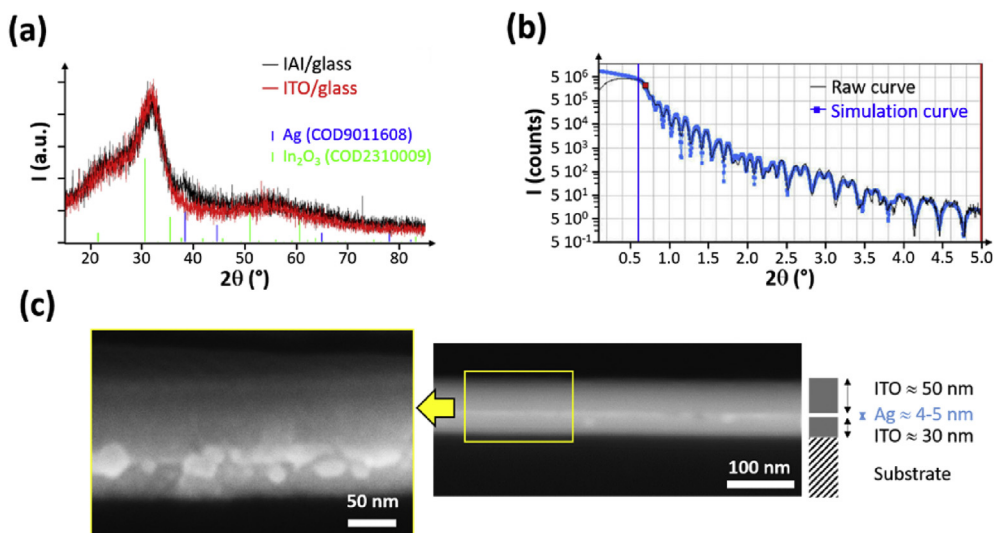


Fig. 2. (a) GI-XRD patterns of the IAI multilayer deposited on glass. Single ITO is also shown for comparison, (b) XRR data and fitted curves of the IAI multilayer. (c) FEG-SEM images of the IAI multilayer in UED and compo modes.

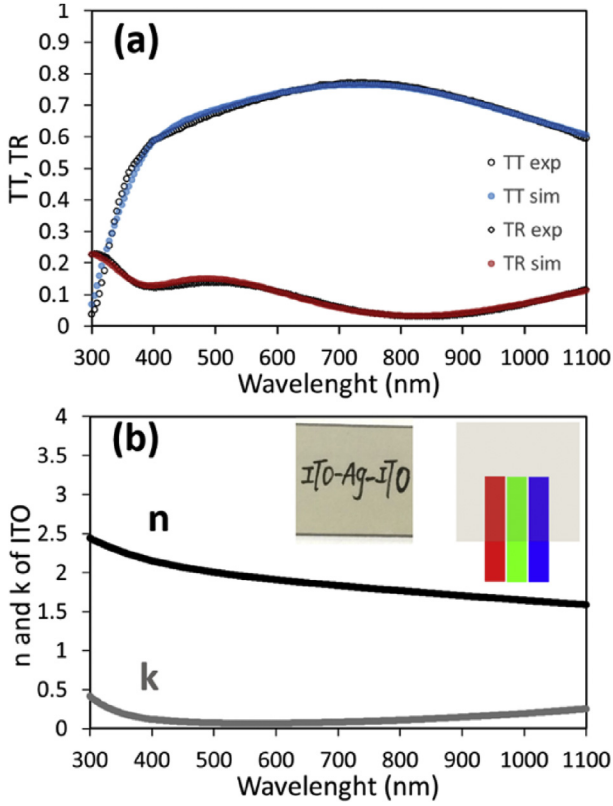


Fig. 3. (a) Total TT and TR experimental (exp) and simulated (sim) spectra of IAI multilayers. (b) n and k optical indexes of ITO deduced from the modulation. A visible model representation and the picture of the real film are inserted for illustration.

stack of 23.5 ± 3 nm of ITO covered with 3.6 ± 2 nm of Ag and a top layer of 64 ± 5 nm of ITO. A colorimetric model representation of all the stacking layers and the corresponding picture of the real film is presented in insert of Fig. 3 (a). This colorimetric representation of the sample allows to represent the true color obtained in transmittance from white light, blue, green and red light without influence of parasite reflectance.

The sheet resistance (R_s directly obtained from the four probe measurement), the luminous transmittance in the visible range (calculated from the data of the full wavelength optical transmittance measured from the 400 nm–780 nm according to Ref. $T_{lum} = \int T(\lambda) f(\lambda) d\lambda / \int f(\lambda) d\lambda$ [4]) and the corresponding figure of merit (calculated with the Haacke's formulae $\Phi_{TC} = T_{lum}^{10} / R_s$ [31]) of the IAI films and the pure ITO film with the same thickness are plotted in Table 2.

The insertion of few nanometers of metallic Ag in the IAI films has a clear effect on the overall sheet resistance with a clear decrease from 47Ω to 7.4Ω (85%) compared with the pure sputtered ITO films. At the same time, the T_{lum} of IAI films only slightly reduces (13%) from 89% to around 77% due to the insert of Ag

Table 2

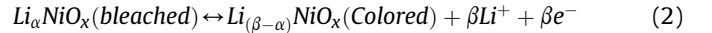
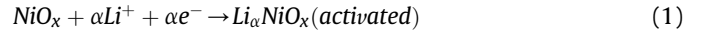
The sheet resistance, luminous transmittance and the figure of merit (Φ_{TC}) of the IAI films and ITO pure films.

Film	Sheet resistance R_s (Ω)	Luminous transmittance T_{lum} (%)	Factor of Merit Φ_{TC} (Ω^{-1})
IAI	7.4	77	9.9×10^{-3}
ITO	47.2	89	6.6×10^{-3}

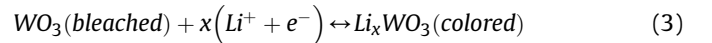
layer. Accordingly, the Haacke's factor of merit largely improves (+50%) from 6.6×10^{-3} to 9.9×10^{-3} due to the insertion of Ag ultra thin layer in the ITO electrode.

3.2. Characterization of the NiO_x and WO_3 films as the IAI films as the electrodes

Electrochromic thin film materials, and in particular the inorganic oxides NiO_x and WO_3 , are among the most promising intelligent materials and have been studied extensively for several years. The color changing NiO_x and WO_3 films is caused by the redox reaction, generally expressing as the double intercalation/extraction of Li^+ ions and electrons on the anode/cathode electrochromic materials. As an example, during the process of the ions extraction, NiO_x films will turn dark brown color [1]. According to the reports [2,20], researchers put forward a simple two step electrochromic reaction scheme to explain the coloration of the anodic electrochromic NiO_x films. Firstly, the activation of NiO_x with the intercalation of lithium corresponds to Eq. (1) [20]. This process can widen the ion channel, which is beneficial to injection and extraction of the Li^+ in the NiO structure leading to a two possible oxidations states of the Ni and a good reversibility (Eq. (2)). The electrochromic Ni^{2+} ions transfer into Ni^{3+} during the coloring process and during the bleaching process, there will be a reverse conversion [20]. Here, e^- presents the electrons.



On the contrary, as the cathode electrochromic material, with the continuous injection of lithium ions, the color of the glass deposited with tungsten oxide changes from colorless to light blue, and gradually deepens with the increase of the voltage, and eventually to dark blue. The WO_3 films turn into dark blue color from the transparent state after the injection of the Li^+ ions due to the partial reduction of the W^{6+} ions into W^{5+} ions. It is called Faughnan model and can be written as Eq. (3) [3].



The thicknesses of the NiO_x (~150 nm) and WO_3 (~610 nm) layers deposited on IAI films were determined from cross section SEM view. The root mean square roughness (R_a) obtained by AFM is 1.64 nm and 2.38 nm, respectively, and remains small enough to avoid any optical haze influence. These characterizations show that the surface morphologies of the NiO_x and WO_3 films deposited on the IAI films are identical to those obtained when deposited on commercial ITO substrates [32–34]. XRD demonstrates that the WO_3 /IAI is similar to those deposited on single ITO substrate (only the characteristic peaks of the ITO and the contribution of the glass substrate are detectable). This is consistent with the literature results whereas minimal temperature of 300 °C is required for the preparation of crystalline WO_3 by magnetron sputtering [35,36]. For the NiO_x /IAI films, only the (111) Bragg's peak of the NiO halite structure is visible at around $2\theta = 37^\circ$ in addition to the ITO and glass contribution.

To explore the electrochromic properties of the NiO_x and WO_3 films deposited on the IAI films, the cyclic voltammetry is used. According to the shape of the curve, the reversible degree of electrode reaction and the charge capacity can be determined. Fig. 4 (a) and (c) display the CV properties and corresponding transmittance at 550 nm of the NiO_x /IAI films which are measured in the same time and Fig. 4 (b) and (d) show that of WO_3 /IAI films. The CV curves shown in Fig. 4 (a) and (b) display that the films can work

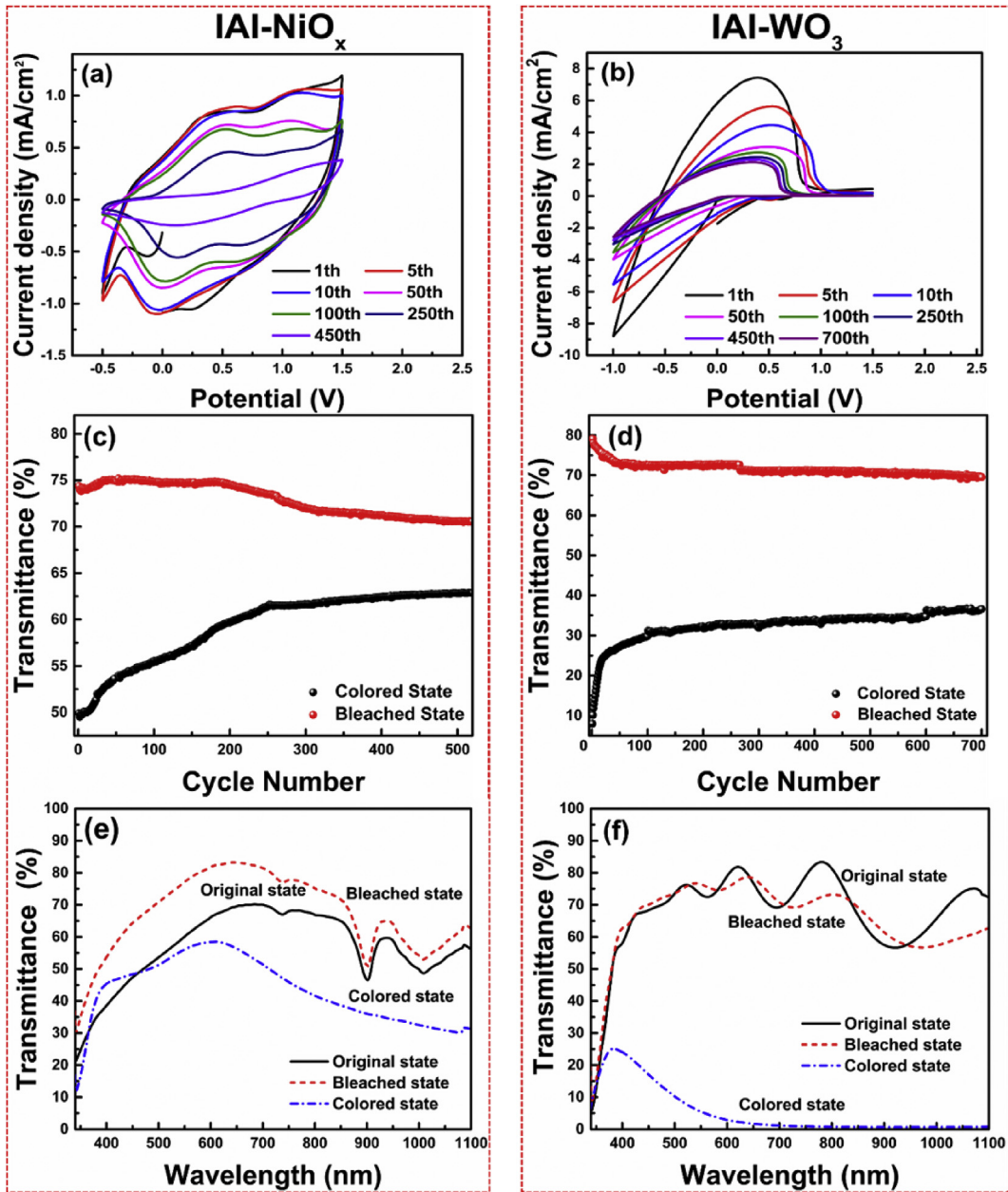


Fig. 4. The CV curves of the (a) NiO_x/IAI and (b) WO_3/IAI films; the rainbow-colored lines refer to the cycle times of the films from the first cycling to the last one. In situ evolutions of transmittance at 550 nm versus cycle number corresponding to the (c) NiO_x and (d) WO_3 films on the IAI substrate. The transmittance of original, bleached and colored state of the new (e) NiO_x/IAI films and (f) WO_3/IAI films under the “full wavelength” mode after one redox reaction.

hundreds of cycles although the capacity decreases with the process of the redox reaction. For the NiO_x/IAI films (Fig. 4 (a)), the current density varies from -1.2 to $+1.2$ mA/cm^2 for the first cycle in the -0.5 to $+1.5$ V potential range and the transmittance of the cycle at 550 nm varies from 48% (the colored state) to 75% (the bleached state). In the case of the WO_3/IAI films (Fig. 4 (b)), the current density varies from -9 to $+8$ mA/cm^2 in the -1 to $+1.5$ V potential range. The optical modulation almost reaches 80% which indicates that the electrode and the electrochromic layer both play an excellent role compared with the single TCO films as electrode in previous work [1,4], whereas the maximum optical modulation of 74% is obtained.

It can be seen in Fig. 4 (c) and (d) that during the first 30 cycles, the NiO_x/IAI films are more stable than the WO_3/IAI films due to its

sharp decrease (from $\Delta T \approx 80\%$ to $\Delta T \approx 44\%$) in term of optical contrast between the bleach and the colored state. From then on, the WO_3/IAI films are almost stable while the coloration depth of NiO_x/IAI films decreases significantly from 50 to 62% transparency during the first 250 cycles and then it tends to level off. The bleaching state of NiO_x/IAI films decreases gradually from 74 to 73% until 250 cycles and also tends to be stable. Actually, the process displayed in the beginning can be seen as the activation process due to the absent of the balance between the inserted and extracted charges between the Li solution and the electrochromic multi layers [2,37–41]. For this process, it is commonly described as the uptake of Li^+ ions which is good for the fast and reversible insertion extraction reactions [39]. The injection and extraction of the ions will cause the change of the tensile or compressive stress of

the films, resulting in cracking or shedding of the film. The implanted ions are limited by the charge layer in the crystal lattice. Therefore, accumulating with the increasing of the number of cycles, the reversibility of the cycle deteriorates leading to the electrochromic performance declining [4,20,32,42]. Fig. 4 (e) and (f) demonstrate the typical variations of the bleached and colored transmittance spectra of the NiO_x/IAI and WO₃/IAI films which are analyzed under the “full wavelength” mode, using the new samples after one redox reaction. From the results, one can see that the change of the optical transmittance among the bleached and colored state of NiO_x films ($\Delta T \approx 30\%$ at 640 nm) is lower than the one of the WO₃ films ($\Delta T \approx 70\%$ at 640 nm). According to the previous work [4], it may result from the low binding force between the NiO_x thin films and the electrode films.

3.3. Characterization of the ECD

The entire ECD was fabricated by the matched NiO_x/IAI and WO₃/IAI films within LiClO₄ PC PMMA polymer electrolyte. Fig. 5 (a) shows 100 CV curves cycled with time. The second cycle of the *in situ* transmittance at 550 nm and the corresponding CV of the ECD is displayed in Fig. 5 (b). Excellent electrochromic films and devices should exhibit rapid switching response which is defined as the time required to reach 90% of the full modulation [43]. The CA measurement is employed to reveal the bleaching (t_b) and the coloring (t_c) response time with the ± 1.5 V potential lasting 20 s for every process. From the NiO_x/IAI and WO₃/IAI single layer t_b and t_c response times (see Supporting Information for details), the ECD response times are calculated ($t_b = 2.06$ s and $t_c = 2.25$ s) (Fig. 5 (c)).

The coloration response time of WO₃ fabricated by LPCVD (CVD at low pressure), reported by D Vernardou, et al. [37], is 43 s with the FTO as the electrode. It is slower response process than the samples in this work ($t_c = 14.6$ s of WO₃/IAI films). This device has real good response times in comparison with ECD equipped with a single ITO layer ($t_b = 2.0$ s, $t_c = 7.0$ s) or single AZO layer ($t_b = 2.54$ s, $t_c = 7.98$ s) as the electrode [1,4]. To explain the optical modulation amplitude of the ECD, the full wavelength transmittance is carried out after the CA measurement. The transmittance change is about 55% at 550 nm (shown in Fig. 5 (d)). Generally speaking, the bleached response time is shorter and easier than the one of the colorations [1,21], due to the lower conductivities of the bleached state forms than those of the colored state forms. The electrochromic response time is determined by the dispersion coefficient of ions and the length of dispersing channels [41,44]. The former is mainly dependent on the chemical and crystal structure of the electrochromic materials, while the latter depends on the microstructure of the electrochromic materials. Therefore, electrochromic efficiency often depends on the surface morphology of the electrochromic materials [45,46].

The safe potential range of ECD is important, therefore, ECD are operated with the continuous changing potential varying as ± 0.5 V, ± 1 V, ± 1.5 V and ± 2 V, respectively. To avoid the activation process of the ECD at the beginning, the 10th cycle is chosen and Fig. 6 (a) shows the CV acquired in various potential. When ± 2 V is applied, there appears a new peak. It is surmised that the large potential during the coloration process may cause some ions trapping in the films which need much larger potential to take them away. This had to be proved in future work. Obviously, as the potential increasing,

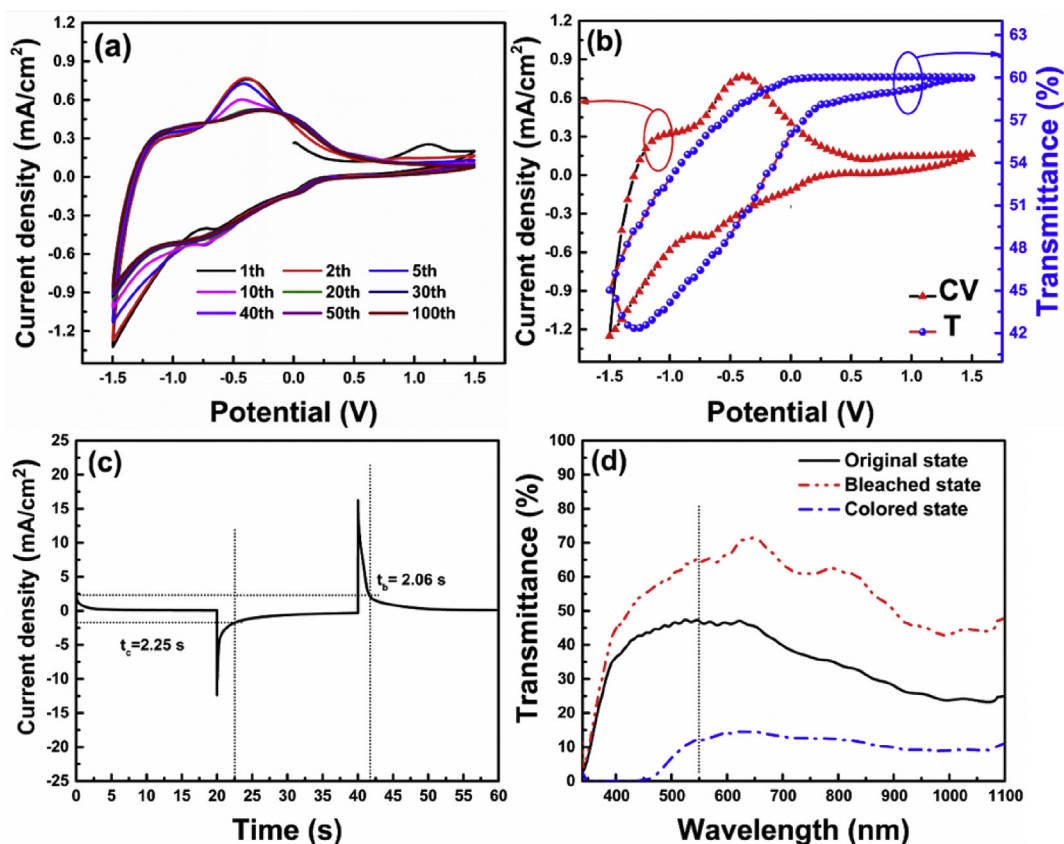


Fig. 5. (a) The CV of the ECD, the rainbow-colored lines refer to the cycle times; (b) *In situ* second transmittance at 550 nm and corresponding CV for the cycle of the laminated ECD with the IAI films as the electrode; (c) the response time of the ECD under CA mode and (d) the original, bleached and colored state of the ECD with the potential of ± 1.5 V lasting 20 s for each process.

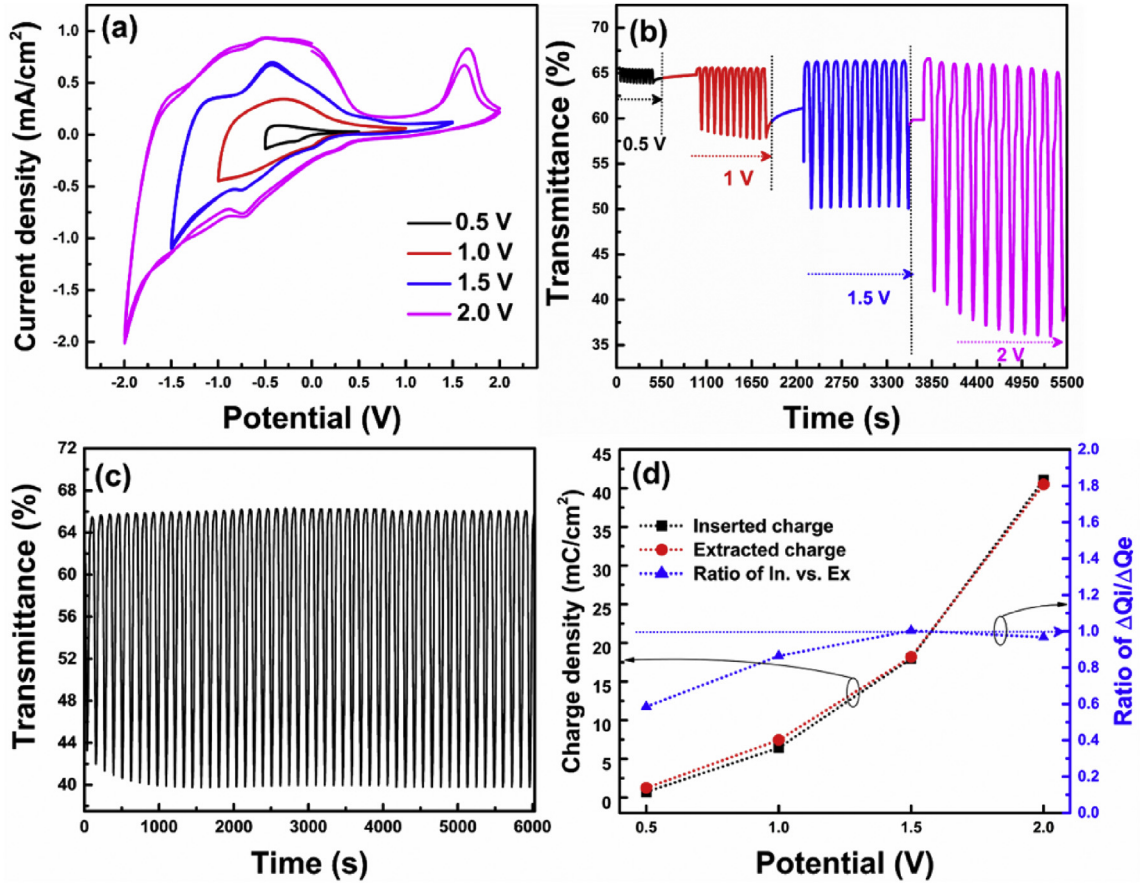


Fig. 6. Electrochemical properties of ECD at various voltage: (a) Variations of 10th CV curves of the ECD at different applied potentials from ± 0.5 V to ± 2 V during coloring processes with a scan rate of 50 mV/s. (b) Dynamic optical transmittance curve of ECD in function of operation potentials from ± 0.5 V to ± 2.0 V at 550 nm. (c) the lifetime of the ECD at 550 nm cycled with the potential ± 2.0 V. (d) the charge density and the ratio of the inserted charge and extracted charge.

the capacity of all the ECD increase. The corresponding in situ optical transmittance at 550 nm continuing to measure after the test of ECD under ± 2.0 V is shown in Fig. 6 (b). With the potential increasing up to ± 2.0 V, the ECD performs well throughout and exhibits good stability up to 6000 cycles (Fig. 6 (c)).

The electrochromic process is related to the Li ion transferring between the electrolyte and the films. As the process is divided into the oxidation and reduction reactions, there exist the inserted and extracted charge density. The charge density is related to the evolution of the capacity and calculated by the area of capacity of the CV curves. Meaningfully, the cathodic (anodic) peak current density of the CV curve is as the function of the Li ion inserted (or extracted). The ratio between the inserted charge density (ΔQ_i) and the extracted charge density (ΔQ_e) presents the ability of the reversibility. If the ratio is close to one, the films occupy a good reversibility [37,47,48]. Therefore, the lithium ion diffusion coefficient (D) is one important parameter to reflect this phenomenon. It can be received by Eq. (4) [49].

$$i_p = 2.72 \times 10^5 \times n^{3/2} \times D^{1/2} \times C_0 \times v^{1/2} \quad (4)$$

where i_p is the peak current density, n is the number of the electrons (assumed to be 1), D is the diffusion coefficient, C_0 is the concentration of the active ions in the solution (1 M), and v is the scan rate of 50 mV/s. According to R.T. Wen et al. [2,3], during the process, there will be some ions or charges trapped in the films bringing about the damage to the films. Calculated by the capacity of the CV, the inserted/extracted charge density and the ratio of

ΔQ_i vs. ΔQ_e are displayed in Fig. 6 (d). It can be seen clearly that the ECD performs good durability, stability, and reversibility.

The coloration efficiency (CE) is also a very important electrochromic properties of ECD and it is associated with the optical density (ΔOD) and the intercalated charges (Q_i) [25,38]. It can be obtained by Eq. (5).

$$CE = \left(\frac{\Delta OD}{Q_i} \right)_{\lambda \ 550nm} \left(\frac{\log(T_b/T_c)}{Q_i} \right)_{\lambda \ 550nm} \quad (5)$$

where the ΔOD is also called absorbance, T_b is the transmittance of the bleached state at 550 nm and T_c is the coloration state's one. According to the previous results, the CE of the ECD is 31.7 cm²/C, which confirms that the multilayer IAI structure is a suitable electrode in the electrochromic process.

4. Conclusion

In conclusion, optimized properties of innovative Electrochromic Device using ITO/Ag/ITO electrodes have been highlighted. The stacked ITO/Ag/ITO films with low resistance and high transparency have been fabricated by DC magnetron sputtering at room temperature. The IAI (50 nm/5 nm/30 nm) films have a sheet resistance as low as 7.4 Ω and the figure of merit (Φ_{TC}) of $9.9 \times 10^{-3} \Omega^{-1}$. As TC electrodes, the IAI films showed excellent behavior in the NiO_x/IAI, WO₃/IAI and full Glass/IAI/NiO_x/LiClO₄ PC PMMA/WO₃/IAI/Glass ECD structure. The ECD displays a wide optical modulation ($\sim 55\%$ at 550 nm), rapid response ($t_b = 2.06$ s and

t_c 2.25 s), good durability (operate stably more than 6000 s) and stability with a coloration efficiency of $31.7 \text{ cm}^2/\text{C}$. The wider potentials during the process lead to a larger transmittance change. The innovative ECD with the IAI films as the electrodes have furtherly expanded the research field of the electrochromism and the use of the DMD structure electrodes for electrochromic devices.

Acknowledgement

The authors would like to acknowledge the financial support of the National Natural Science Foundation of China (No. KZ73095501), the National Natural Science Foundation of China (No. KZ73086401), China Scholarship Council (CSC, Grant No. 201706020126, M.Y. WANG), the Academic Excellence Foundation of BUAA for PhD Students (Mengying WANG, BY1419138), the National Natural Science Foundation of China (No. 61775131), and the Fundamental Research Funds for the Central Universities (No. KG12050101, ZG216S18A9, ZG226S18M9). Authors acknowledge S. Le Blond du Plouy from UMS Castaing, Université de Toulouse for providing the FEG SEM characterization.

Appendix A. Supplementary data

Supplementary data to this article can be found online at <https://doi.org/10.1016/j.electacta.2019.01.184>.

References

- [1] M. Wang, X. Diao, G. Dong, Y. He, Q. Liu, Optical, electrical, and electrochemical properties of indium tin oxide thin films studied in different layer-structures and their corresponding inorganic all-thin-film solid-state electrochromic devices, *J. Vac. Sci. Technol. A* 35 (2) (2017) 21512. <https://doi.org/10.1116/1.4975823>.
- [2] R.T. Wen, C.G. Granqvist, G.A. Niklasson, Anodic electrochromism for energy-efficient windows: Cation/anion-based surface processes and effects of crystal facets in nickel oxide thin films, *Adv. Funct. Mater.* 25 (22) (2015) 3359–3370. <https://doi.org/10.1002/adfm.201500676>.
- [3] R.-T. Wen, C.G. Granqvist, G.A. Niklasson, Eliminating degradation and uncovering ion-trapping dynamics in electrochromic WO₃ thin films, *Nat. Mater.* 14 (10) (2015) 996–1001. <https://doi.org/10.1038/nmat4368>.
- [4] M. Wang, Q. Liu, G. Dong, Y. He, X. Diao, Influence of thickness on the structure, electrical, optical and electrochromic properties of AZO thin films and their inorganic all-solid-state devices, *Electrochim. Acta* 258 (2017) 1336–1347. <https://doi.org/10.1016/j.electacta.2017.11.192>.
- [5] G.A. Niklasson, C.G. Granqvist, Electrochromics for smart windows: thin films of tungsten oxide and nickel oxide, and devices based on these, *J. Mater. Chem.* 17 (2) (2007) 127–156. <https://doi.org/10.1039/B612174H>.
- [6] Y. Kim, S. Park, S. Kim, B.K. Kim, Y. Choi, J.H. Hwang, H.J. Kim, Flash lamp annealing of indium tin oxide thin-films deposited on polyimide backplanes, *Thin Solid Films* 628 (2017) 88–95. <https://doi.org/10.1016/j.tsf.2017.03.016>.
- [7] A. El Hichou, A. Kachouane, J.L. Bubendorff, M. Addou, J. Ebothe, M. Troyon, A. Bougrine, Effect of substrate temperature on electrical, structural, optical and cathodoluminescent properties of In₂O₃-Sn thin films prepared by spray pyrolysis, *Thin Solid Films* 458 (1–2) (2004) 263–268. <https://doi.org/10.1016/j.tsf.2003.12.067>.
- [8] C. Chen, Z. Wang, K. Wu, H. Ye, Tunable near-infrared epsilon-near-zero and plasmonic properties of Ag-ITO co-sputtered composite films, *Sci. Technol. Adv. Mater.* 19 (1) (2018) 174–184. <https://doi.org/10.1080/14686996.2018.1432230>.
- [9] H. Taha, Z.-T. Jiang, D.J. Henry, A. Amri, C.-Y. Yin, A.B. Alias, X. Zhao, Improved mechanical properties of sol-gel derived ITO thin films via Ag doping, *Mater. Today Commun.* 14 (December 2017) (2018) 210–224. <https://doi.org/10.1016/j.mtcomm.2017.12.009>.
- [10] A.H. Ali, Z. Hassan, A. Shuhaimi, Enhancement of optical transmittance and electrical resistivity of post-annealed ITO thin films RF sputtered on Si, *Appl. Surf. Sci.* 443 (2018) 544–547. <https://doi.org/10.1016/j.apsusc.2018.03.024>.
- [11] M. Kumar, B. Singh, P. Yadav, V. Bhatt, M. Kumar, K. Singh, J.-H. Yun, Effect of structural defects, surface roughness on sensing properties of Al doped ZnO thin films deposited by chemical spray pyrolysis technique, *Ceram. Int.* 43 (4) (2017) 3562–3568. <https://doi.org/10.1016/j.ceramint.2016.11.191>.
- [12] P. Dhamodharan, C. Manoharan, M. Bououdina, R. Venkatchalapathy, S. Ramalingam, Al-doped ZnO thin films grown onto ITO substrates as photoanode in dye sensitized solar cell, *Sol. Energy* 141 (2017) 127–144. <https://doi.org/10.1016/j.solener.2016.11.029>.
- [13] G. Lee, M. P. M. W. Park, J. Kim, Enhanced Optical and Electrical Properties of ITO/Ag/AZO Transparent Conductors for Photoelectric Applications, *Int. J. Photoenergy* 2017 (2017). Article ID 8315802, 9 pages, <https://doi.org/10.1155/2017/8315802>.
- [14] N. Akin Sonmez, M. Donmez, B. Comert, S. Ozcelik, Ag/M-seed/AZO/glass structures for low-E glass: Effects of metal seeds, *Int. J. Appl. Glass Sci.* June (2017) 1–9. <https://doi.org/10.1111/ijag.12331>.
- [15] J.A. Jeong, H.K. Kim, Low resistance and highly transparent ITO Ag ITO multilayer electrode using surface plasmon resonance of Ag layer for bulk-heterojunction organic solar cells, *Sol. Energy Mater. Sol. Cells* 93 (10) (2009) 1801–1809. <https://doi.org/10.1016/j.solmat.2009.06.014>.
- [16] S. Boscarino, I. Crupi, S. Mirabella, F. Simone, A. Terrasi, TCO/Ag/TCO transparent electrodes for solar cells application, *Appl. Phys. A* 116 (2014) 1287 (2014). <https://doi.org/10.1007/s00339-014-8222-9>.
- [17] H. Li, Y. Lv, X. Zhang, X. Wang, X. Liu, High-performance ITO-free electrochromic films based on bi-functional stacked WO₃/Ag/WO₃ structures, *Sol. Energy Mater. Sol. Cells* 136 (2015) 86–91. <https://doi.org/10.1016/j.solmat.2015.01.002>.
- [18] Y. Liu, Y. Lv, Z. Tang, L. He, X. Liu, Highly stable and flexible ITO-free electrochromic films with bi-functional stacked MoO₃/Ag/MoO₃ structures, *Electrochim. Acta* 189 (2016) 184–189. <https://doi.org/10.1016/j.electacta.2015.12.115>.
- [19] W. Dong, Y. Lv, L. Xiao, Y. Fan, N. Zhang, X. Liu, Bifunctional MoO₃/WO₃/Ag/MoO₃ WO₃ films for efficient ITO free electrochromic devices, *ACS Appl. Mater. Interfaces* 8 (49) (2016) 33842–33847. <https://doi.org/10.1021/acsami.6b12346>.
- [20] Q. Liu, G. Dong, Y. Xiao, M.P. Delplancke-Ogletree, F. Reniers, X. Diao, Electrolytes-relevant cyclic durability of nickel oxide thin films as an ion-storage layer in an all-solid-state complementary electrochromic device, *Sol. Energy Mater. Sol. Cells* 157 (2016) 844–852. <https://doi.org/10.1016/j.solmat.2016.07.022>.
- [21] M. Da Rocha, Y. He, X. Diao, A. Rougier, Influence of cycling temperature on the electrochromic properties of WO₃/NiO devices built with various thicknesses, *Sol. Energy Mater. Sol. Cells* (2018) 57–65. <https://doi.org/10.1016/j.solmat.2017.05.070>.
- [22] P.Y. Pennarun, S. Papaefthimiou, P. Yianoulis, P. Jannasch, Electrochromic devices operating with electrolytes based on boronate ester compounds and various alkali metal salts, *Sol. Energy Mater. Sol. Cells* 91 (4) (2007) 330–341. <https://doi.org/10.1016/j.solmat.2006.09.009>.
- [23] J. Wang, E. Khoo, P.S. Lee, J. Ma, Synthesis, assembly and electrochromic properties of uniform crystalline WO₃ nanorods, *J. Phys. Chem. C* 112 (37) (2008) 14306–14312. <https://doi.org/10.1021/jp804035r>.
- [24] D. Ma, J. Wang, Inorganic electrochromic materials based on tungsten oxide and nickel oxide nanostructures, *Sci. China Chem.* 60 (1) (2017) 54–62. <https://doi.org/10.1007/s11426-016-0307-x>.
- [25] F. Zhang, G. Dong, J. Liu, S. Ye, X. Diao, Polyvinyl butyral-based gel polymer electrolyte films for solid-state laminated electrochromic devices, *Ionics* 23 (7) (2017) 1879–1888. <https://doi.org/10.1007/s11581-017-1996-y>.
- [26] W. Theiss, Hard & Software. <http://www.mtheiss.com>.
- [27] S.W. Liu, T.H. Su, P.C. Chang, T.H. Yeh, Y.Z. Li, L.J. Huang, C.F. Lin, ITO-free, efficient, and inverted phosphorescent organic light-emitting diodes using a WO₃/Ag/WO₃ multilayer electrode, *Org. Electron.* 31 (2016) 240–246. <https://doi.org/10.1016/j.orgel.2016.01.035>.
- [28] S.K. O'Leary, S.R. Johnson, P.K. Lim, The relationship between the distribution of electronic states and the optical absorption spectrum of an amorphous semiconductor: An empirical analysis, *J. Appl. Phys.* 82 (7) (1997) 3334–3340. <https://doi.org/10.1063/1.365643>.
- [29] M.S. Farhan, E. Zalmezhad, A.R. Bushroa, A.A. Daa Sarhan, *Int. J. Precis. Eng. Manuf.* 14 (2013) 1465. <https://doi.org/10.1007/s12541-013-0197-5>.
- [30] F. Zhu, K. Zhang, C.H.A. Huan, A.T. Shen Wee, E. Guenther, S.J. Chua, Effect of ITO Carrier Concentration on the Performance of Organic Light-Emitting Diodes, *MRS Online Proc. Library Archive* 598 (1999), in: <http://doi.org/10.1557/PROC-598-BB11.11>.
- [31] C.-C. Wu, Highly flexible touch screen panel fabricated with silver-inserted transparent ITO triple-layer structures, *RSC Adv.* 8 (22) (2018) 11862–11870. <https://doi.org/10.1039/C7RA13550E>, 2018, <https://doi.org/10.1039/C7RA13550E>.
- [32] X. Song, G. Dong, F. Gao, Y. Xiao, Q. Liu, X. Diao, Properties of NiOx and its influence upon all-thin-film ITO/NiOx/LiTaO₃/WO₃/ITO electrochromic devices prepared by magnetron sputtering, *Vacuum* 111 (2015) 48–54. <https://doi.org/10.1016/j.vacuum.2014.09.007>.
- [33] M. Kiristi, F. Bozduman, A. Gulec, E. Teke, L. Oksuz, A.U. Oksuz, H. Deligoz, Complementary all Solid State Electrochromic Devices Using Carboxymethyl Cellulose Based Electrolytes, *J. Macromol. Sci. C* 51 (6) (2014) 481–487. <https://doi.org/10.1080/10601325.2014.906258>.
- [34] A. Llordés, G. Garcia, J. Gazquez, D.J. Milliron, Tunable near-infrared and visible-light transmittance in nanocrystal-in-glass composites, *Nature* 500 (7462) (2013) 323–326. <https://doi.org/10.1038/nature12398>.
- [35] Y. Wei, M. Chen, W. Liu, L. Li, Y. Yan, Electrochemical investigation of electrochromic devices based on NiO and WO₃ films using different lithium salts electrolytes, *Electrochim. Acta* 247 (2017) 107–115. <https://doi.org/10.1016/j.electacta.2017.07.016>.
- [36] M.H. Kim, H.W. Choi, K.H. Kim, Properties of WO₃-x Electrochromic Thin Film Prepared by Reactive Sputtering with Various Post Annealing Temperatures, *Jpn. J. Appl. Phys.* 52 (11S) (2013) 11NB09. <http://iopscience.iop.org/1347-4065/52/11S/11NB09>.
- [37] D. Vernardou, K. Psifis, D. Louloudakis, G. Papadimitropoulos, D. Davazoglou,

- N. Katsarakis, E. Koudoumas, Low Pressure CVD of Electrochromic WO₃ at 400 °C, *J. Electrochem. Soc.* 162 (9) (2015) H579–H582. <https://doi.org/10.1149/2.0281509jes>.
- [38] Q. Liu, G. Dong, Q. Chen, J. Guo, Y. Xiao, M.P. Delplancke-Ogletree, X. Diao, Charge-transfer kinetics and cyclic properties of inorganic all-solid-state electrochromic device with remarkably improved optical memory, *Sol. Energy Mater. Sol. Cell.* 174 (April 2017) (2018) 545–553. <https://doi.org/10.1016/j.solmat.2017.09.012>.
- [39] R.J. Mortimer, D.R. Rosseinsky, P.M.S. Monk, Electrochromic Materials and Devices: present and future, *Electrochromic Mater Dev.* 77 (2015) 1–638. <https://doi.org/10.1002/9783527679850>.
- [40] H. Farsi, Z. Barzgari, The lithiation studies of nanostructured tungsten oxide film prepared via electrochemical precipitation, *Ionics* 19 (10) (2013) 1349–1357. <https://doi.org/10.1007/s11581-013-0865-6>.
- [41] S.H. Lee, H.M. Cheong, C.E. Tracy, A. Mascarenhas, Alternating current impedance and Raman spectroscopic study on electrochromic a-WO₃ films, *Appl. Phys. Lett.* 76 (26) (2000) 3908–3910. <https://doi.org/10.1063/1.126817>.
- [42] Q. Liu, Q. Chen, Q. Zhang, Y. Xiao, X. Zhong, G. Dong, K. Baert, In situ electrochromic efficiency of a nickel oxide thin film: origin of electrochemical process and electrochromic degradation †, *J. Mater. Chem. C* 12 (2018). <https://doi.org/10.1039/C7TC04696K>.
- [43] C. Yan, W. Kang, J. Wang, M. Cui, X. Wang, C.Y. Foo, P.S. Lee, Stretchable and wearable electrochromic devices, *ACS Nano* 8 (1) (2014) 316–322. <https://doi.org/10.1021/nn404061g>.
- [44] S.H. Lee, R. Deshpande, P. Parilla, K. Jones, B. To, A. Mahan, et al., Crystalline WO₃ nanoparticles for highly improved electrochromic applications, *Adv. Mater.* 18 (6) (2006) 763–766. <https://doi.org/10.1002/adma.200501953>.
- [45] C.G. Granqvist, E. Avendano, A. Azens, Electrochromic coatings and devices: Survey of some recent advances, *Thin Solid Films* 442 (1–2) (2003) 201–211. [https://doi.org/10.1016/S0040-6090\(03\)00983-0](https://doi.org/10.1016/S0040-6090(03)00983-0).
- [46] C.G. Granqvist, Electrochromic tungsten oxide films: Review of progress 1993–1998, *Sol. Energy Mater. Sol. Cell.* 60 (3) (2000) 201–262. [https://doi.org/10.1016/S0927-0248\(99\)00088-4](https://doi.org/10.1016/S0927-0248(99)00088-4).
- [47] P.R. Bueno, C. Gabrielli, H. Perrot, Coloring ionic trapping states in WO₃ and Nb₂O₅ electrochromic materials, *Electrochim. Acta* 53 (17) (2008) 5533–5539. <https://doi.org/10.1016/j.electacta.2008.03.004>.
- [48] A. Avendano, A. Azens, G.A. Niklasson, C.G. Granqvist, Sputter deposited electrochromic films and devices based on these: Progress on nickel-oxide-based films, *Mater. Sci. Eng. B-ADV* 138 (2) (2007) 112–117. <https://doi.org/10.1016/j.mseb.2005.07.029>.
- [49] P.S. Patil, P.R. Patil, S.S. Kamble, S.H. Pawar, Thickness-dependent electrochromic properties of solution thermolyzed tungsten oxide thin films, *Sol. Energy Mater. Sol. Cell.* 60 (2) (2000) 143–153. [https://doi.org/10.1016/S0927-0248\(99\)00079-3](https://doi.org/10.1016/S0927-0248(99)00079-3).